Electromagnetic Wave Propagation in an Externally Modulated Low-Pass Transmission Line

José Roberto Reyes-Ayona and Peter Halevi

***Abstract*— We present a novel concept of a modulated transmission line: a low-pass dynamic transmission line (DTL) whose capacitors are replaced by varactors that are externally modulated in tandem. The modulation voltages are periodic in time and identical in all the unit cells (and there is no pump wave). Accurate modeling leads to two bands, $\beta_1(\omega)$ and $\beta_2(\omega)$ for the propagation constant, separated by a gap $\Delta\beta$. We have fabricated an eight-cell DTL and measured $\beta_{1,2}(\omega)$ for a range of frequencies of the signal wave up to the modulation frequency $f_M = 310$ MHz, finding very good agreement between the experimental and theoretical results. These are also compared with an effective medium description, with the dynamic permittivity $\varepsilon(t)$ being equal to the distributed capacitance $C(t)/a$ at every instant t and the permeability μ equal to the distributed inductance L/a, where a is the size of the unit cell. There is good agreement for long wavelengths, $\beta a \lesssim 1$, including the β-gap, which, for negligible resistive effects, is proportional to the modulation strength. Such gaps are characteristic of periodicity in time of a parameter and were predicted for "temporal photonic crystals." We have also confirmed experimentally that for every frequency f, a harmonic of frequency $f_M - f$ is excited, giving rise to beats when $f \cong f_M/2$. We expect these experimental and theoretical results to open a new platform for useful applications.**

***Index Terms*— Active circuits, capacitors, dielectric constant, eigenvalues and eigenfunctions, low-pass filters, microwave circuits, microwave propagation, phase measurement, propagation, RLC circuits, transmission line measurements, varactors, waves.**

I. Introduction

WAVE propagation in transmission lines has been the subject of study for many decades. In the 1960s, traveling-wave amplifiers (TWPAs) were widely studied after Cullen [1] showed that parametric excitation of an electric oscillatory circuit was possible and that any method of periodically varying the capacitance or the inductance could be used. In a series of works, Cassedy [2], [4], [5] and Cassedy and Oliner [3] researched the dispersion relations of TWPAs, finding forbidden bands for the imaginary part of the propagation constant βa and discussing the harmonics of the modulation frequency.

Prior to semiconductor amplifiers (which are less complex and have lower noise), TWPAs were very popular and improvements were achieved in the bandwidth, gain, and noise level [6], [7]. Nevertheless, high-quality-factor varactors have low power consumption and are highly tunable. For these reasons, their manufacturing improved UHF applications [8] and they can be used to amplify parametrically large signals [9]. Recently, a dynamic low-pass filter employing varactors in a CMOS process has been simulated to be used as a frequency divider and as a parametric amplifier [10]. In 2015, a time-varying transmission line with varactor diodes was implemented and proposed as a circulator device that allows transmission and reception of signals at the same time and the same frequency [11].

Also, Kozyrev *et al.* [12] achieved parametric amplification in distributed high-pass transmission lines that exhibited metamaterial behavior. Employing (nonlinear) varactors, they also reported harmonic and subharmonic generation, modulated instabilities, and envelope solitons [13]. Further, English *et al.* [14] showed experimentally and numerically that stable localized modes can be produced in a nonlinear bandpass transmission line. Gorkunov and Lapine [15] studied a metamaterial slab composed of an array of split-ring resonators tuned by an external microwave magnetic field.

The modulated or dynamic transmission line (DTL) presented in this paper differs from the TWPA in an important aspect: the propagating pump wave is replaced by uniform or in tandem modulation. That is to say, the capacitance in all unit cells is the same periodic function $C(t)$. A former publication was based on a hypothetic lossless DTL with time-periodic shunt capacitances, however, without specifying the source of modulation [16]. Now, a DTL can be represented as an effective medium if electromagnetic (EM) waves propagating in this medium and in the DTL obey the same dispersion relation $\omega(\beta)$. This occurs in the long-wavelength limit $\beta a \ll 1$, where the distributed capacitance and inductance can be described in terms of an effective permittivity and permeability, respectively. Previously, it was found that the dispersion relation for such a dynamic medium with periodic permittivity $\varepsilon(t)$ is periodic in ω and that there are forbidden bands for the phase constant β [17]. Very recently, we reported the first experimental observation of such a band-gap in a DTL [18]. Further, we showed that a dynamic-periodic slab gives rise to harmonics of the modulation frequency in the reflected and transmitted light [17], that parametric resonances in the response are obtained under appropriate conditions [19], and that in some cases, pulses of harmonics can traverse the slab faster than light in vacuum [20].

We suppose that all the above-listed effects [17], [19], [20] can be reproduced in DTLs. In addition, it is expected that DTLs could be used not only as parametric amplifiers and

Manuscript received December 31, 2015; revised June 30, 2016 and August 16, 2016; accepted August 19, 2016. This work was supported by CONACYT under Project 103644-F. The work of J. R. Reyes-Ayona was supported by CONACYT under Scholarship 317142.

The authors are with the Instituto Nacional de Astrofísica, Óptica y Electrónica, Tonantzintla, Puebla 72840, México (e-mail: ayonarey@hotmail.com; halevi@inaoep.mx).

Color versions of one or more of the figures in this paper are available online at http://ieeexplore.ieee.org.

Digital Object Identifier 10.1109/TMTT.2016.2604319

frequency converters but also as controllable delay lines. A 2-D DTL could separate and route composite signals that are omnipresent in modern communications. Other applications associated with the forbidden β-bands are also possible. Moreover, the working frequency can range from kilohertz to terahertz using split-ring resonators.

In Section II-A, we present a realistic model for our DTL that includes losses as well as explicit modulation sources that feed the nonlinear varactors. In continuation, in Section II-B, we derive the differential equation for the nodal voltage from Kirchhoff's laws applied to the aforementioned model. In Section II-C, we present a perturbational solution for the traveling wave and the eigenvalue equation that describes the dispersion relation for the DTL. Next, in Section II-D, we show that in the long-wavelength limit, neglecting resistance effects, propagation in the DTL can be described by an effective medium. In Section II-E, an approximate analytical solution is presented to show that the propagation constant forms two bands $\beta_1(\omega)$ and $\beta_2(\omega)$ that are separated by a bandgap. Subsequently, in Section II-F, we solve numerically the eigenvalue equation for a realistic model and compare the resulting band structure with that for the approximate analytical solution of Section II-E. After that, in Section III, we describe in detail the fabricated DTL, the measurement of the dispersion relation $\beta(\omega)$, and its comparison to theoretical band structures. Finally, in Section IV, we present conclusions.

II. Modeling, Theory, and Theoretical Results

A. Realistic Modeling of the Externally Modulated Transmission Line

A DTL can be implemented using microstrip technology. A microstrip consists of a dielectric substrate with a ground level copper layer at the bottom and a copper line at the top. The microstrip has a capacitance and an inductance per unit length and their values can be modified inserting lumped elements. The modulation in time can be achieved by means of varactors, which are solid-state devices whose capacitance can be regulated by a dc voltage. However, such a capacitance can become time dependent, if the voltage governing it has an ac component. Indeed, the capacitances of the DTL are controlled by an ac voltage and a dc voltage for inverse polarization. In this paper, the voltage applied to the varactors is harmonic, namely, $V_\Omega(t) = \bar{V}_\Omega[1 + m\sin(\Omega t)]$. Here, $\bar{V}_\Omega$ is the inverse polarization voltage and $\Omega/2\pi \equiv f_M$ and m are, respectively, the modulation frequency and strength (or briefly, "modulation") of the ac voltage.

A realistic description of the DTL requires considering not only the modulation voltage $V_\Omega(t)$ but also a finite conductivity for the microstrip copper line, modeled as a series resistance R, substrate losses modeled as a shunt conductance G, a current leakage through the modulation feeding lines corresponding to the resistance R_Ω, and a parasitic capacitance C_P associated with the microstrip (which cannot be modulated). The resistance R_Ω experienced by the propagating wave has to be chosen high, so as to avoid current flow through the voltage source (which would diminish the modulation intensity m).

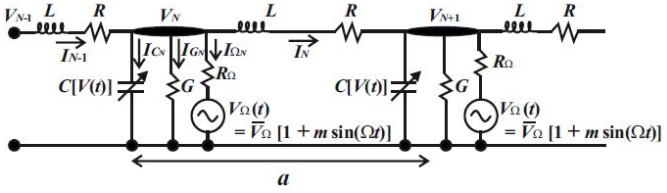

Fig. 1. Low-pass DTL unit cell of length a between nodes N and $N+1$. The voltages $V_\Omega(t)$ have the same amplitude and phase at all nodes. As a result, the capacitances $C[V(t)]$ are modulated in tandem and the voltage difference $V_N - V_{N+1}$ is given by only the small signal voltage of frequency ω of the traveling wave.

On the other hand, the modulating current should "see" a very small resistance in order to have a negligible voltage drop over the resistance R_Ω in comparison with $V_\Omega(t)$. This ensures that the nodal voltage is approximately given by the modulation voltage, as explained in the Appendix. The unit cell of the DTL is shown in Fig. 1 along with the currents and voltages at the nodes N and $N+1$.

If the capacitance is voltage dependent, then the ac current through such a capacitor is

$$I(t) = \frac{dQ}{dt} = \frac{d}{dt}[C(V)V(t)]. \tag{1}$$

It follows that

$$I(t) = \left\{C[V(t)] + \frac{dC}{dV}V(t)\right\}\frac{dV}{dt}. \tag{2}$$

Thus, we see that because of the dependence of C on V, the current is not determined by the capacitance itself, but rather by the expression in the curly brackets, which we name *dynamic capacitance*, being of interest only if the current and voltage are time dependent. Other expressions such as incremental capacitance, differential capacitance, and junction capacitance are also used. A negative capacitance effect has been observed in semiconductor devices [21].

For convenience, we include the parasitic capacitance C_P in our definition of the dynamic capacitance

$$\tilde{C}(V) = C(V) + \frac{dC}{dV}V + C_P. \tag{3}$$

Then the current through a varactor is simply

$$I_C(t) = \tilde{C}[V(t)]\frac{dV}{dt}. \tag{4}$$

The dependences of the dynamic and conventional capacitances on applied voltage are shown in Fig. 2. It is significant that unlike the conventional capacitance $C(V)$, the dynamic capacitance can be negative for a range of voltages, as seen in Fig. 2.

B. Derivation of Differential Equation for the Nodal Voltage

Applying Kirchhoff's current law to node N in Fig. 1, we have

$$I_{N-1} - I_N = I_{C_N} + I_{G_N} + I_{\Omega_N}. \tag{5}$$

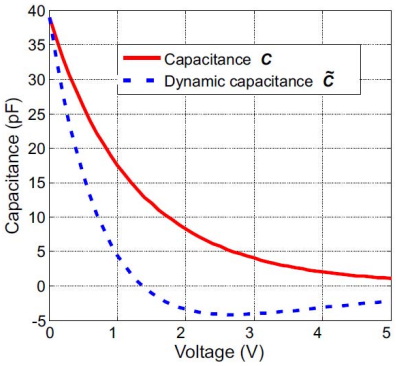

Fig. 2. Conventional and dynamic capacitances as a function of applied voltage for the varactor diodes in the DTL.

Next, we apply the operator Ld/dt to the last equation

$$L\frac{d(I_{N-1})}{dt} - L\frac{d(I_N)}{dt} = L\frac{d(I_{C_N})}{dt} + L\frac{d(I_{G_N})}{dt} + L\frac{d(I_{\Omega_N})}{dt}. \tag{6}$$

Using Kirchhoff's voltage law, the voltage difference between nodes can be expressed in terms of the resistance R, the inductance L, and the corresponding currents as

$$V_{N-1} - V_N = L\frac{d(I_{N-1})}{dt} + RI_{N-1} \tag{7a}$$

$$V_N - V_{N+1} = L\frac{d(I_N)}{dt} + RI_N. \tag{7b}$$

The currents associated with the resistance R_Ω and the conductance G on node N are given by

$$I_{\Omega_N} = (V_N - V_\Omega)/R_\Omega \tag{8a}$$

and

$$I_{G_N} = GV_N. \tag{8b}$$

According to (4), the current through the varactor is

$$I_{C_N} = \tilde{C}(V_N)dV_N/dt. \tag{8c}$$

With the help of (5), (7), and (8) and with the abbreviation$G_R = G + 1/R_\Omega$, (6) can be rewritten as

$$V_{N-1} + V_{N+1} - 2V_N - R\tilde{C}(V_N)\frac{dV_N}{dt} - RG_RV_N - L\frac{d}{dt}\left[\tilde{C}(V_N)\frac{dV_N}{dt}\right] - LG_R\frac{dV_N}{dt} = -\frac{R}{R_\Omega}V_\Omega - \frac{L}{R_\Omega}\frac{dV_\Omega}{dt}. \tag{9}$$

In the next section, we will proceed to solve this equation for the signal voltage wave.

C. Perturbational Solution for the Signal Wave and the Eigenvalue Equation

The nodal voltage $V_N(t)$ is composed of the voltage $U_\Omega(t)$, approximately equal to the modulation voltage $V_\Omega(t)$ for a sufficently small resistance R_Ω (see the Appendix) and the voltage $v_N(t)$ of the traveling (signal) wave

$$V_N(t) = U_\Omega(t) + v_N(t). \tag{10}$$

We also assume that the latter voltage is much smaller than the former

$$|v_N(t)| \ll U_\Omega(t) \tag{11}$$

so that the varactor modulation is mostly due to the modulation voltage. The capacitance as a function of nodal voltage can be then written approximately as the first two terms of a Taylor series

$$\tilde{C}(V_N) = \tilde{C}(U_\Omega) + \tilde{C}'(U_\Omega)v_N(t) \tag{12}$$

where the prime implies differentiation with respect to the argument. The small signal voltage on node N can be expressed as $v_N(t) = v(t)e^{j\beta aN}$. It follows that

$$v_{N\pm1}(t) = v_N(t)e^{\pm j\beta a}. \tag{13}$$

Equations (10) and (13) imply that the first three terms of (9) are proportional to $v_N(t)$ [$U_\Omega(t)$ canceling out]

$$\begin{aligned} V_{N-1} + V_{N+1} - 2V_N &= v_{N-1} + v_{N+1} - 2v_N \\ &= (e^{-j\beta a} + e^{j\beta a} - 2)v_N \\ &= 2(\cos\beta a - 1)v_N. \end{aligned} \tag{14}$$

Substituting (10), (12), and (14) in (9) (and omitting the index N on v_N), we obtain a differential equation for $v(t)$ of the form (see the Appendix)

$$S(t)\frac{d^2v(t)}{dt^2} + T(t)\frac{dv(t)}{dt} + U(t)v(t) = F(t). \tag{15}$$

The functions $S(t)$, $T(t)$, $U(t)$, and $F(t)$ all being periodic with the period $1/f_M = 2\pi/\Omega$, the left-hand side of this equation can only have terms that are proportional to $\exp[j(n\Omega - \omega)t]$ (associated with the traveling wave of frequency $f = \omega/2\pi$), while the right-hand side can only have terms proportional to $\exp(jn\Omega t)$ (associated with the modulation in the absence of a wave). Hence, (15) can be satisfied at every instant of time only if its two sides vanish independently and identically. As shown in the Appendix, the requirement $F(t) = 0$ leads to the conclusion that $U_\Omega(t) \cong V_\Omega(t)$ if the resistance R_Ω is sufficiently small (as satisfied experimentally).

We then turn to the homogeneous differential equation obtained by replacing the right-hand side of (15) by zero. One solution has the form of a temporal Bloch–Floquet wave, namely, a harmonic oscillation $e^{-j\omega t}$ with a periodically modulated amplitude $\sum_n \tilde{v}_n e^{jn\Omega t}$

$$\tilde{v}(t) = \sum_n \tilde{v}_n e^{j(n\Omega-\omega)t}. \tag{16}$$

Substitution in (15) with $F(t) = 0$ gives

$$\begin{aligned} &\sum_m S_m e^{jm\Omega t}\sum_n \tilde{v}_n(jn\Omega - j\omega)^2 e^{j(n\Omega-\omega)t} \\ &\quad + \sum_m T_m e^{jm\Omega t}\sum_n \tilde{v}_n(jn\Omega - j\omega)e^{j(n\Omega-\omega)t} \\ &\quad + \sum_m U_m e^{jm\Omega t}\sum_n \tilde{v}_n e^{j(n\Omega-\omega)t} = 0 \end{aligned} \tag{17}$$

where $S(t)$, $T(t)$, and $U(t)$ have been expanded in Fourier series.

It follows that

$$\sum_m \sum_n [U_m + T_m(jn\Omega - j\omega) + S_m(jn\Omega - j\omega)^2]\tilde{v}_n \times e^{j(m+n)\Omega t} = 0. \quad (18)$$

This will be satisfied at all times provided that

$$\sum_n [U_{m-n} + j(n\Omega - \omega)T_{m-n} - (n\Omega - \omega)^2 S_{m-n}]\tilde{v}_n = 0. \quad (19)$$

Because U_{m-n} depends on β, this is an eigenvalue equation that determines the dispersion relation $\omega(\beta)$.

D. Effective Medium Description

In this section, we show that for waves of long wavelength $2\pi/\beta$ in comparison with the period a, propagation in the DTL can be described by an effective medium approximation. We also neglect all mechanisms of absorption ($R = 0$, $G = 0$, and $R_\Omega = \infty$), thus replacing $U_\Omega(t)$ by $V_\Omega(t)$ in (A.3). With $F(t) = 0$ and $\beta a \ll 1$, (15) then becomes

$$L\tilde{C}(V_\Omega)\frac{d^2v}{dt^2} + 2L\tilde{C}'(V_\Omega)\dot{V}_\Omega(t)\frac{dv}{dt} + [\beta^2 a^2 + L\tilde{C}'(V_\Omega)\ddot{V}_\Omega(t) + L\tilde{C}''(V_\Omega)\dot{V}_\Omega^2(t)]v(t) = 0. \quad (20)$$

This can be rewritten as

$$\frac{L}{a}\frac{\tilde{C}(V_\Omega)}{a}\frac{d^2v}{dt^2} + 2\frac{L}{a}\frac{d}{dt}\left[\frac{\tilde{C}(V_\Omega)}{a}\right]\frac{dv}{dt} + \left\{\beta^2 + \frac{L}{a}\frac{d^2}{dt^2}\left[\frac{\tilde{C}(V_\Omega)}{a}\right]\right\}v(t) = 0 \quad (21)$$

or, compactly, as

$$\frac{L}{a}\frac{d^2}{dt^2}\left\{\frac{\tilde{C}(V_\Omega)}{a}v(t)\right\} + \beta^2 v(t) = 0. \quad (22)$$

Comparing (22) with the wave equation for a plane wave propagating in a dielectric medium of dynamic permittivity $\varepsilon(t)$ and permeability μ (=const), it has been derived in [17], although with the assumption that $\mu = \mu_0$ (the vacuum permeability). The generalization to $\mu \neq \mu_0$ is straightforward and reads

$$\mu\frac{d^2}{dt^2}\{\varepsilon(t)E(t)\} + \beta^2 E(t) = 0. \quad (23)$$

From the comparison, we then conclude that the properties of a voltage wave propagating in a DTL are identical to the properties of an EM wave that propagates in a dielectric ("effective") medium provided that

$$\tilde{C}[V_\Omega(t)]/a = \varepsilon(t), \quad \text{for all } t \quad (24a)$$

$$L/a = \mu \quad (24b)$$

$$\beta a \ll 1 \quad (24c)$$

and that losses are

We note that in this section, no particular model has been assumed for the varactor, that is, the function $\tilde{C}(V_\Omega)$ is arbitrary. Moreover, neither has the form of the temporal modulation been restricted, and thus $V_\Omega(t)$ is not necessarily a periodic function as far as (24a) is concerned.

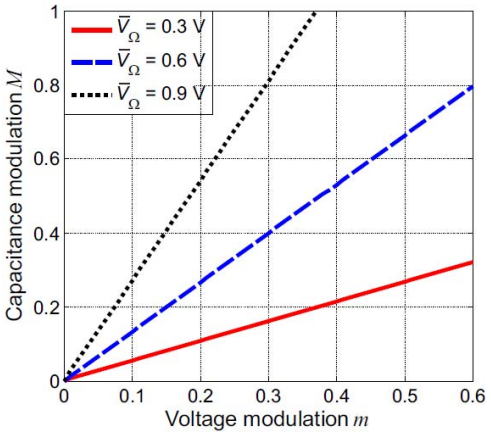

Fig. 3. Capacitance modulation M versus voltage modulation m, according to (28) for three values of the polarization voltage $\bar{V}_\Omega$.

E. Linear Modeling of the Varactor and the Approximation of Weak Modulation

In this section, we will solve the eigenvalue equation (19) analytically, subject to appropriate approximations. The purpose is to show that two bands are obtained for the propagation constant, $\beta_1(\omega)$ and $\beta_2(\omega)$, and that these bands are separated by a bandgap that is proportional to the modulation m. A linear approximation for the dynamic capacitance suffices if $m \ll 1$

$$\tilde{C}(V) = \tilde{C}(\bar{V}) + (d\tilde{C}/d\bar{V})(V - \bar{V}). \quad (25)$$

We also assume harmonic modulation

$$V_\Omega(t) = \bar{V}_\Omega(1 + m\sin\Omega t). \quad (26)$$

With the abbreviations $\tilde{C}(\bar{V}) = \tilde{C}$ and $d\tilde{C}/d\bar{V} = \tilde{C}'$, (25) becomes

$$\tilde{C}(\bar{V}_\Omega, t) = \tilde{C} + \tilde{C}'\bar{V}_\Omega m\sin\Omega t \quad (27)$$

or

$$\tilde{C}(\bar{V}_\Omega, t) = \tilde{C}(1 + M\sin\Omega t) \quad M = \tilde{C}'\bar{V}_\Omega m/\tilde{C}. \quad (28)$$

Then the only nonvanishing Fourier components in (19) are

$$S_0 = L\tilde{C} \quad S_{\pm1} = \mp(j/2)ML\tilde{C} \quad (29a)$$

$$T_0 = LG_R + R\tilde{C} \quad T_{\pm1} = M\tilde{C}(\Omega L \mp jR/2) \quad (29b)$$

$$U_0 = 4\sin^2(\beta a/2) + RG_R \quad U_{\pm1} = M\tilde{C}\Omega(R \pm j\Omega L)/2. \quad (29c)$$

Fig. 3 shows how the modulation M of the dynamic capacitance $\tilde{C}(t)$ can be quite different from the modulation m of the voltage $V_\Omega(t)$, as described by (28). In the case of weak modulation, the important harmonics are $n = 0$ and $n = 1$. This follows from the *empty lattice model* of periodicity [22] applied to temporal modulation of the capacitance. We will then restrict the values of m and n in (19) to 0 or 1. This results in the two homogeneous equations

$$(U_0 - j\omega T_0 - \omega^2 S_0)\tilde{v}_0 + [U_{-1} + j(\Omega - \omega)T_{-1} - (\Omega - \omega)^2 S_{-1}]\tilde{v}_1 = 0$$
$$(U_1 - j\omega T_1 - \omega^2 S_1)\tilde{v}_0 + [U_0 + j(\Omega - \omega)T_0 - (\Omega - \omega)^2 S_0]\tilde{v}_1 = 0. \quad (30)$$

The determinant of the coefficients of $\tilde{v}_0$ and $\tilde{v}_1$ must vanish, and hence,

$$(U_0 - j\omega T_0 - \omega^2 S_0)(U_0 + j(\Omega-\omega)T_0 - (\Omega-\omega)^2 S_0) - (U_1 - j\omega T_1 - \omega^2 S_1)(U_{-1} + j(\Omega-\omega)T_{-1} - (\Omega-\omega)^2 S_{-1}) = 0. \quad (31)$$

It is easy to see that this leads to a quadratic equation for $\sin^2(\beta a/2)$ and, therefore, two bands $\beta_1(\omega)$ and $\beta_2(\omega)$. These are plotted in Section II-F and are compared with the "exact" band structure. The closest approach between these bands occurs at the frequency $\omega = \Omega/2$, to which we restrict the calculation that follows. Substitution of (31) in (29) leads to the approximate result [assuming $(2R/\Omega L)^2 \ll 1$]

$$4\sin^2(\beta a/2) = \tilde{\Omega}^2/4 - RG_R \pm (\tilde{\Omega}^2/8) \times [M^2 - 16(G_R/\Omega\tilde{C} + R/\Omega L)^2]^{1/2}$$
$$G_R = G + 1/R_\Omega. \quad (32)$$

Here, we defined the normalized circular frequency (for $\tilde{C} > 0$) as

$$\tilde{\Omega} = \Omega\sqrt{L\tilde{C}}. \quad (33)$$

First, we analyze the lossless case, with $R = G = 0$ and $R_\Omega \to \infty$. Then we can express (32) compactly as

$$2\sin(\beta_\pm a/2) = (\tilde{\Omega}/2)(1 \pm M/2)^{1/2}. \quad (34)$$

This equation has two solutions for β, provided that $(\tilde{\Omega}/4)(1 + M/2)^{1/2} \le 1$. Therefore, having assumed weak modulation ($M \ll 1$) in this section, the parameter $\tilde{\Omega}$ cannot be greater than 4. That is to say, if $\tilde{\Omega} > 4$, no propagation can take place in the DTL for frequencies $\omega \simeq \Omega/2$. This establishes the important characteristic of a periodically modulated DTL that there are two bands, $\beta_-(\omega)$ or $\beta_1(\omega)$ and $\beta_+(\omega)$ or $\beta_2(\omega)$, separated by a *β-gap* whose width is proportional to the modulation.

In the long-wavelength limit $\beta a \ll 1$, (34) becomes

$$\beta_\pm a \simeq (\tilde{\Omega}/2)(1 \pm M/2)^{1/2} \quad (35)$$

and with $\beta_\pm \simeq \bar{\beta} \pm \Delta\beta/2$, the forbidden bandgap is

$$\Delta\beta a \simeq \tilde{\Omega}M/4 \quad M \ll 1 \quad (36)$$

or

$$\Delta\beta/\bar{\beta} \simeq M/2. \quad (37)$$

Thus, in this approximation, the normalized gap depends only on the modulation of the capacitors.

Returning to consider the resistances R, $1/G$, and R_Ω, (32) can be rewritten as

$$4\sin^2(\beta a/2) = (\tilde{\Omega}^2/4) - RG_R \pm (\tilde{\Omega}^2/8)\left[M^2 - M_R^2\right]^{1/2} \quad (38)$$

where

$$M_R = 4(G_R/\Omega\tilde{C} + R/\Omega L). \quad (39)$$

According to (38), there are three possible behaviors for the phase constant values βa.

1) $M > M_R$: The square root is real, so that the phase constant values are real, $\beta_+ \neq \beta_-$, and there is a bandgap $\Delta\beta = \beta_+ - \beta_-$. In the approximation considered, two undamped waves propagate.
2) $M = M_R$: Now $\beta_+ = \beta_- = \bar{\beta}$, and the solution reduces to
$$2\sin(\beta a/2) \simeq (\tilde{\Omega}/2)(1 - 2RG_R/\tilde{\Omega}^2). \quad (40)$$
Hence, the two β-bands now touch at $\omega = \Omega/2$ and there is no β-gap. Only a single wave propagates.
3) $M < M_R$: The square root is imaginary, so approximately
$$4\sin^2(\beta a/2) \cong (\tilde{\Omega}^2/4) \pm j(\tilde{\Omega}^2/8)\left(M_R^2 - M^2\right)^{1/2}. \quad (41)$$

This has solutions of the form $\beta = \beta'(1 \pm j\kappa)$, where β' and κ are real and $\kappa \ll 1$. If $\beta a \ll 1$, considering that the first term on the right-hand side is much larger than the second term, we have

$$\beta a \simeq (\tilde{\Omega}/2)\left[1 + (j/4)\left(M_R^2 - M^2\right)^{1/2}\right]. \quad (42)$$

Here, we have selected the physically correct sign of the square root (+) that gives rise to attenuation. A single damped wave propagates.

F. Numerical Results for the Electromagnetic Band Structure

In the previous section, a linear model was considered for the dynamic capacitance of the varactors. Now, we proceed to very accurate modeling and present the resulting dispersion curves. The dynamic capacitance is described by the quadratic expansion

$$\tilde{C}(V) = \tilde{C} + \tilde{C}'(V - \bar{V}) + \frac{1}{2}\tilde{C}''(V - \bar{V})^2. \quad (43)$$

With harmonic modulation (26), this becomes

$$\tilde{C}(V) = \tilde{C} + \tilde{C}M\sin\Omega t + \tilde{C}''\bar{V}_\Omega^2 m^2 \sin^2(\Omega t)/2 \quad (44)$$

where the capacitance modulation M has been defined in (28) and its relation with m is shown in Fig. 3 for the varactor of Fig. 2.

The only nonvanishing Fourier components of (A.3a)–(A.3c) are

$$S_0 = L(\tilde{C} + Q) \quad S_{\pm1} = \mp jL\tilde{C}M/2 \quad S_{\pm2} = -LQ/2 \quad (45a)$$

$$T_0 = LG_R + R(\tilde{C} + Q) \quad T_{\pm1} = \tilde{C}M(\Omega L \mp jR/2) \quad (45b)$$

$$T_{\pm2} = -Q(R/2 \pm j2\Omega L) \quad U_0 = 4\sin^2(\beta a/2) + RG_R \quad (45c)$$

$$U_{\pm1} = \Omega\tilde{C}M(R \pm j\Omega L)/2 \quad U_{\pm2} = \Omega Q(2\Omega L \mp jR) \quad (45d)$$

where

$$Q = \tilde{C}''\bar{V}_\Omega^2 m^2/4 \quad \tilde{C}'' = d^2\tilde{C}(V)/d\bar{V}^2. \quad (46)$$

Using (45), we solved numerically (19) and compared the results with the ones obtained by the approximate dispersion relation given by (31). Figs. 4–8 show the dispersion curves

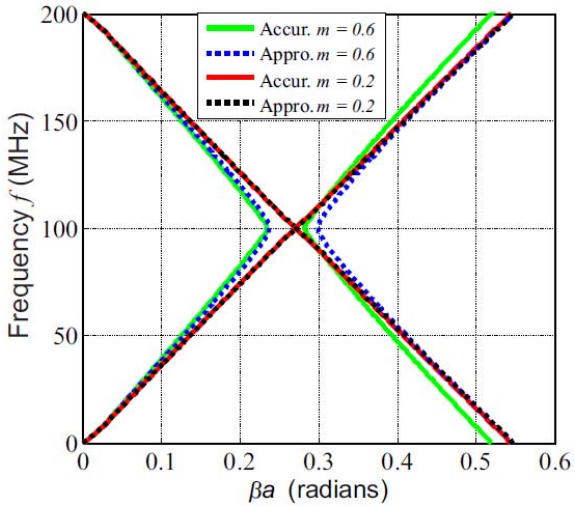

Fig. 4. Accurate and approximate dispersion relations for two values of the voltage modulation strength m. The solutions have excellent agreement for the weak modulation ($m = 0.2$), but the approximate band structure is not accurate for the second β band for $m = 0.6$. The parameter values are $R_\Omega = 800\ \Omega$, $G = 0.001$ S, $R = 0.24\ \Omega$, $\bar{V}_\Omega = 0.6$ V, and $f_M = 200$ MHz.

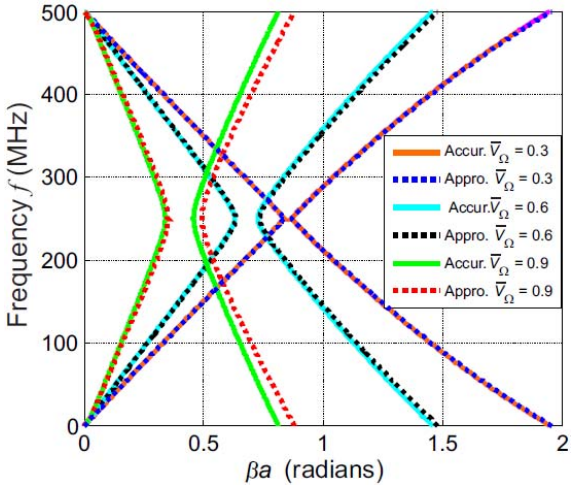

Fig. 5. Accurate and approximate dispersion relations for three values of the polarization voltage $\bar{V}_\Omega$. The modulation intensity and resistances are the same for all curves. Capacitance values depend on $\bar{V}_\Omega$, and as a consequence, they are different for each voltage value. The parameters are $R_\Omega = 800\ \Omega$, $G = 0.001$ S, $R = 0.24\ \Omega$, $m = 0.3$, and $f_M = 500$ MHz.

for the accurate and the approximate solutions for two values of modulation. For Figs. 4–8., the inductance value $L = 11.85$ nH. As expected, the forbidden bandgap is directly associated with the modulation intensity m.

Fig. 5 shows the dispersion relations for three values of the polarization voltage $\bar{V}_\Omega$. The approximate solution describes extremely well the DTL dispersion relation, failing only for the second band in the case of $\bar{V}_\Omega = 0.9$ V. Because this solution is not limited to small values of the phase constant βa, it can mimic well the accurate solution even for $\beta a \gtrsim 1$. In Fig. 5, the voltage modulation has the same value $m = 0.3$, but the capacitance modulation values are different for each value of $\bar{V}_\Omega$: $M = 0.16$ for $\bar{V}_\Omega = 0.3$, $M = 0.39$ for $\bar{V}_\Omega = 0.6$, and $M = 0.81$ for $\bar{V}_\Omega = 0.9$. As a consequence, there is not

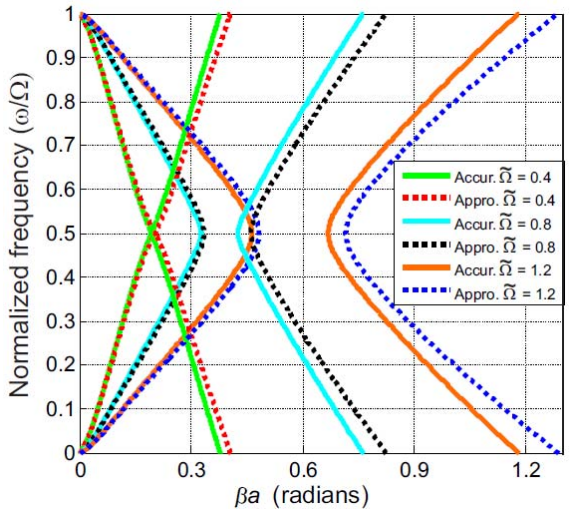

Fig. 6. Accurate and approximate dispersion relations for three values of the normalized modulation frequency $\tilde{\Omega}$. All the other parameters of the DTL are identical: $R_\Omega = 800\ \Omega$, $G = 0.001$ S, $R = 0.34\ \Omega$, $m = 0.3$, and $\bar{V}_\Omega = 0.9$ V.

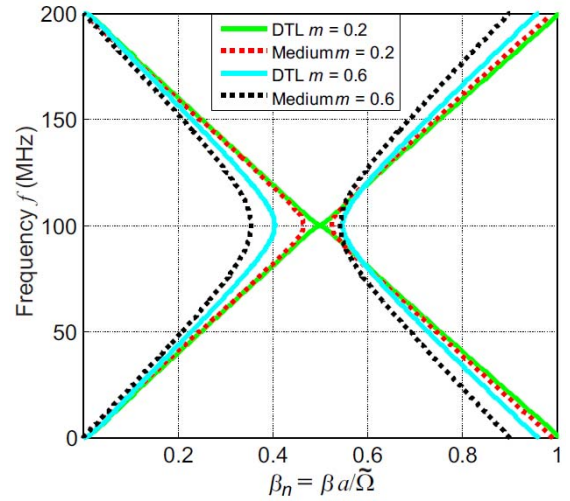

Fig. 7. Band structures are compared for the DTL and the effective medium for two values of the modulation m. Bandgaps are larger for the effective medium due to neglect of losses. The parameters are $R_\Omega = 2000\ \Omega$, $G = 0.001$ S, $R = 0.04\ \Omega$, $\bar{V}_\Omega = 0.6$ V, $f_M = 200$ MHz, and $\tilde{\Omega} = 0.53$.

even a bandgap for $\bar{V}_\Omega = 0.3$ even though the associated phase constant is larger due to a bigger capacitance, but there is a bandgap for $\bar{V}_\Omega = 0.9$ while the corresponding βa values are the smallest.

Fig. 6 presents the dispersion relations for different values of the normalized modulation frequency $\tilde{\Omega}(= \Omega(L\tilde{C})^{1/2})$. The dispersion curves are qualitatively different from those in Fig. 5. In Fig. 5, the wider bandgap occurs at small values of the phase constant, while in Fig. 6, this happens for larger values of βa. In Fig. 6, three different values of $\tilde{\Omega}$ are considered. The capacitance modulation M needed to overcome losses, in order to have a bandgap, is frequency dependent and it decreases as the modulation frequency Ω increases (and the value of $\tilde{\Omega}$ augments), as shown in Fig. 6.

We developed realistic modeling of a DTL, based on (19), as well as an approximate treatment, according to (32).

TABLE I

COMPARISON OF ACCURATE SOLUTIONS OF (19) AND APPROXIMATE SOLUTIONS OF (32) FOR THE DTL. HERE, $R = 0.12\ \Omega$, $R_\Omega = 2000\ \Omega$, $G = 0.001$ S, AND $\bar{V}_\Omega = 0.6$ V

$\tilde{\Omega}$	M	$\bar{\beta}a$		$\Delta\beta a$		$\Delta\beta/\bar{\beta}$	
		App.	Accur	Approx	Accur	Approx.	Accur
0.4	0.4	0.2002	0.1978	0.0	0.0	0.0	0.0
0.4	0.5	0.1996	0.1958	0.0204	0.0119	0.1022	0.0608
0.4	0.6	0.1991	0.1934	0.0396	0.0325	0.1989	0.1680
0.6	0.4	0.3002	0.2965	0.0394	0.0366	0.1312	0.1234
0.6	0.5	0.2993	0.2936	0.0605	0.0566	0.2021	0.1928
0.6	0.6	0.2983	0.2899	0.0792	0.0734	0.2655	0.2532
0.8	0.4	0.4016	0.3962	0.0673	0.0648	0.1676	0.1636
0.8	0.5	0.4000	0.3922	0.0914	0.0874	0.2285	0.2228
0.8	0.6	0.3986	0.3873	0.1144	0.1080	0.2870	0.2789
1.2	0.4	0.6068	0.5991	0.1168	0.1139	0.1925	0.1901
1.2	0.5	0.6051	0.5931	0.1508	0.1455	0.2492	0.2453
1.2	0.6	0.6031	0.5856	0.1844	0.1755	0.3058	0.2997

This approximation gives good insight into the behavior of the DTL for relatively large values of the parameter $\tilde{\Omega}$, as seen in Table I. From Table I, we can appreciate that $\bar{\beta}a$ is well given by the approximation $\tilde{\Omega}/2$ [see (35)] regardless of the modulation M. On the other hand, in the last two columns, another rough approximation, $\Delta\beta/\bar{\beta} \simeq M/2$ [see (37)] is reasonable only for $\tilde{\Omega} = 0.8$ and 1.2. This is due to the fact that resistances are neglected in (35)–(37), and as Ω (and therefore $\tilde{\Omega}$) increase, losses become less important [see (39)]. Regarding the comparison between accurate and approximate solutions, this is quite good for $\tilde{\Omega} = 0.6$, 0.8, and 1.2, but fails for $\tilde{\Omega} = 0.4$ (even though both solutions take into account losses). The reason for this is that in (32), the approximation $(2R/\Omega L)^2 \ll 1$ is not well satisfied for small $\tilde{\Omega}$.

Now we compare the dispersion relations for the DTL and the effective medium. Because losses have not been considered for the effective medium, there is no good agreement for the bandgap width. Fig. 7 shows the dispersion relations for two values of m, with the phase constant replaced by $\beta_n = \beta a/\tilde{\Omega}$. Taking into account (24), $\beta_n = \beta/\Omega(\mu\bar{\varepsilon})^{1/2}$ for the effective medium is independent of the period a. Fig. 8 presents the DTL and effective medium dispersion relations for three values of $\tilde{\Omega}$. There is a very good correspondence for values of the normalized phase constant β_n smaller than about 0.5.

III. EXPERIMENT, EXPERIMENTAL RESULTS, AND COMPARISON OF EXPERIMENTAL AND THEORETICAL BAND STRUCTURES

First, we discuss the components needed for the experiment. A DTL with eight 5-mm cells was fabricated using microstrip

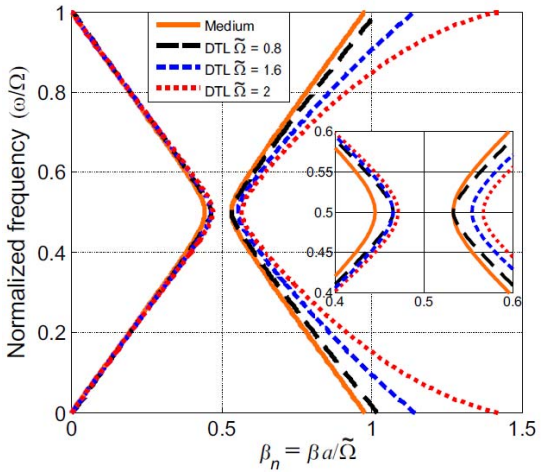

Fig. 8. Dispersion curves for the DTL and effective medium for three values of the normalized circular frequency $\tilde{\Omega}$. Here, $R_\Omega = 2000\ \Omega$, $G = 0.001$ S, $R = 0.04\ \Omega$, $\bar{V}_\Omega = 0.6$ V, and $m = 0.3$.

technology on an RT Duroid 5880 substrate with the following characteristics: dielectric constant $= 2.2 \pm 0.02$, dissipation factor $(\tan\delta) = 0.0009$, dielectric thickness $= 1.575$ mm, and copper layer thickness $= 35\ \mu$m. Commercial inductors of 1 mm $\times$ 0.5 mm were inserted in the DTL, with an inductance of 10 nH in the internal cells and an inductance of 5 nH in the cells at the ends. An SMV1249 hyperabrupt union varactor from Skyworks of 1.6 mm $\times$ 0.8 mm was inserted in each cell. The capacitance–voltage relation for this varactor is shown in Fig. 2. There are seven vias of 0.5 mm to ground at each varactor ground level to guarantee good grounding. Besides the DTL, we also used the following.

1) Eight bandpass filters with a central frequency of 310 MHz and a fractional bandwidth of 5.6%. Each bandpass filter is based on a miniaturized ring resonator [23] of 16 mm $\times$ 16 mm fabricated on an RT Duroid 6010.2LM substrate with dielectric constant $= 10.7$, $\tan\delta = 0.0023$, and dielectric thickness $= 1.27$ mm.
2) Eight matched amplifiers with an RFMD's InGaP HBT MMIC amplifier using coplanar technology.
3) Two 50-Ω coaxial power splitters 4 way-0° ZN4PD1-63W+.
4) Two 50-Ω coaxial power splitters 2 way-0° ZX10R-14+.
5) Four low-pass filters with a cutoff frequency of 260 MHz.
6) Low-loss 50-Ω coaxial cables.

Fig. 9 shows a photograph of the fabricated DTL.

The experimental setup (shown in Fig. 10) was as follows. The dc inverse polarization voltage was provided by a single dc voltage source through an ac blocking network, ensuring that $\bar{V}_\Omega$ [and consequently $\tilde{C}(\bar{V})$] is the same for all varactors. The modulation voltage signal of 310 MHz was obtained from a signal generator Anritsu MG3692C and then with the combination of one two-way splitter and two four-way splitters, divided into eight equal voltage signals. Every divided signal then passed through the amplifiers and was

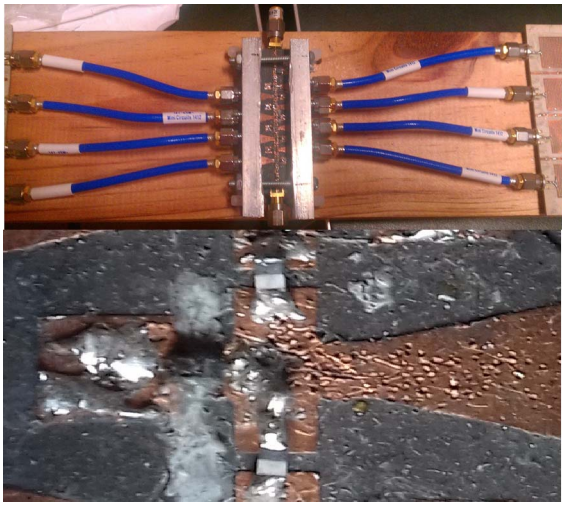

Fig. 9. Photograph of the 63 mm × 25.2 mm fabricated eight-cell DTL, including feeding lines, ac blocking network, dc blocking capacitors, and coupling impedances for the modulation lines. SMA connectors were used. A single cell is also shown.

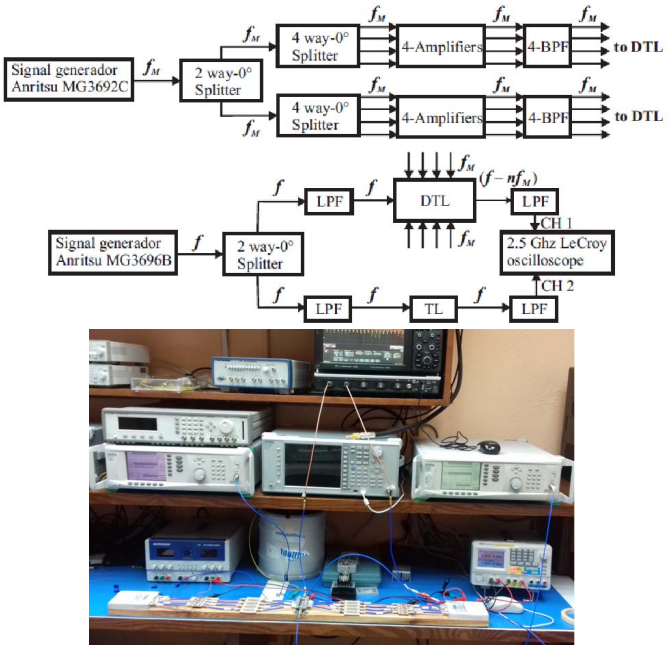

Fig. 10. Block diagram of the experimental setup (and a photograph), where LPF indicates low-pass filter, BPF means bandpass filter, CH stand for oscilloscope channel, and TL includes feeding lines, ac blocking network, unmodulated cells at its ends, and connectors that are also present at the DTL.

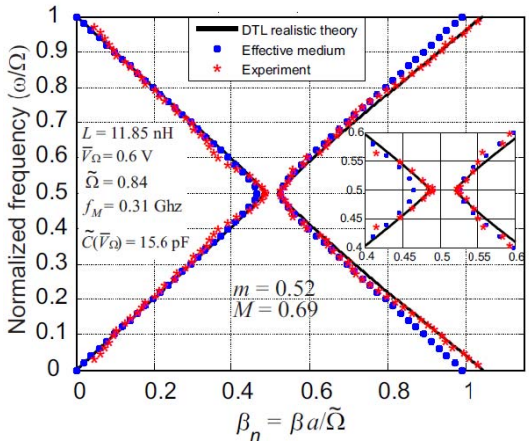

Fig. 11. Theoretical (solid line) and experimental (asterisks) dispersion relations, along with that for the corresponding effective medium (dots) for $m = 0.52$. Inset: zoomed-in view of the forbidden phase constant band. Such a gap in β-bands obtains only if $m > m_{\min} = 0.39$ (38 and 39). Here, $R = 0.23\ \Omega$, $G = 0.001$ S, and $R_\Omega = 800\ \Omega$.

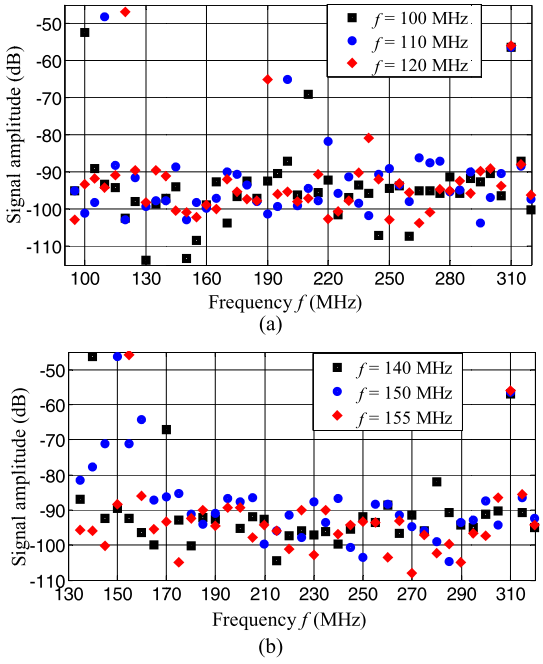

Fig. 12. Spectra of the recovered signals at the end of the DTL for six externally launched voltage signals of varying frequencies f, where harmonics $f_M - f$ are also present. The peaks at $f_M = 310$ MHz all have the same amplitude confirming that the modulation intensity is the same for all the externally launched signal frequencies and that the modulation voltage at all the nodes is the same $V_\Omega(t)$ as explained in the Appendix. Here, $L = 11.85$ nH, $G = 0.001$ S, $\bar{V}_\Omega = 0.6$ V, and $m = 0.5$ when: (a) $f = 100$, 110, and 120 MHz and (b) $f = 140$, 150, and 155 MHz.

amplified. In continuation, each of these signals went through a bandpass filter and was then applied at each cell varactor in order to be modulated. A low-pass filter, used to filter the 310-MHz modulation voltage and higher frequency harmonics, was placed at each end of the DTL. The traveling-wave signal of frequency f was generated from a signal generator Anritsu MG3696B and then divided by a two-way splitter into two halves. One half went right through the DTL, while the other half, used as a back-to-back reference measurement, went from end to end of the transmission line with identical connectors, feeding lines, dc blocking capacitors, ac blocking network, and low-pass filters at its ends as the DTL. The two signals were then simultaneously recovered, displayed, and stored on a 2.5-GHz LeCroy oscilloscope. Digital signal processing was then performed on the stored signals allowing them to be separated into individual phase shift components ($\beta_1 a$, $\beta_2 a$, …). The phase constant is $8\omega\Delta_t$ and Δ_t is the time difference between the transmitted wave and reference wave. The process is then repeated for different values of f (from 10 to 305 MHz) and the dispersion relation is obtained.

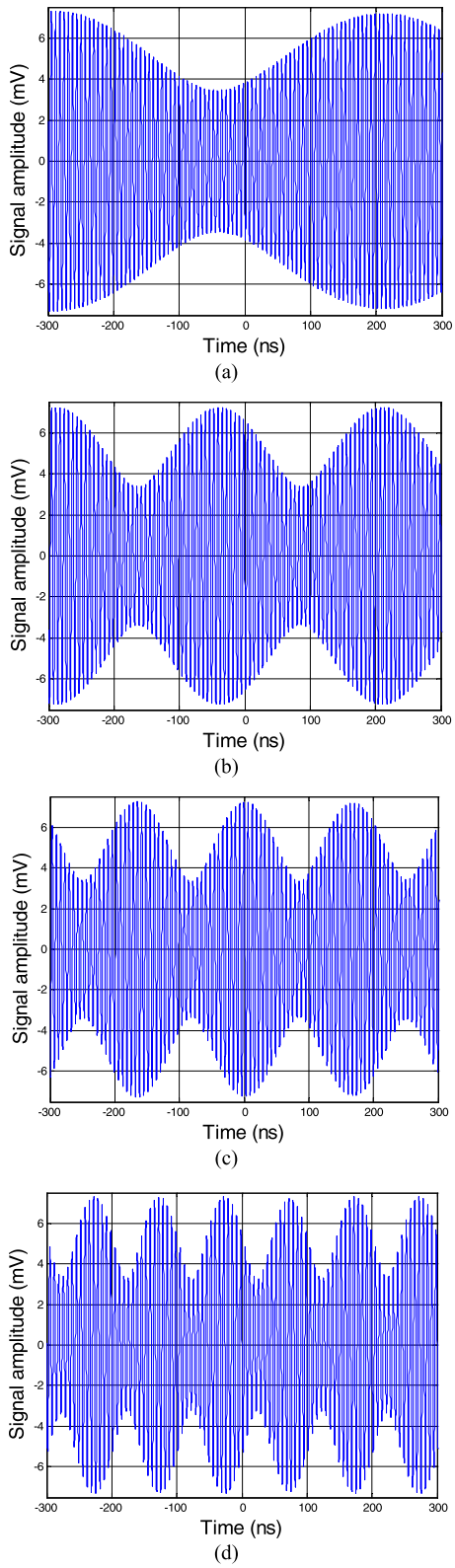

Fig. 13. Recovered signals at the end of the DTL after digital signal processing where there is an envelope signal of lower frequency, corresponding to beats. The externally launched traveling waves have frequencies (a) 154, (b) 153, (c) 152, and (d) 150 MHz. Here, $L = 11.85$ nH, $G = 0.001$ S, and $\bar{V}_\Omega = 0.3$ V.

The resulting experimental dispersion relation for voltage modulation of $m = 0.52$ and normalized phase constant $\beta_n = \beta a/\tilde{\Omega}$ [$=\beta/\Omega(\mu\bar{\varepsilon})^{1/2}$] is shown in Fig. 11. It is compared with the band structures obtained from the "realistic theory" of the DTL (Section II-F) and the effective medium treatment (Section V). There is excellent agreement between the three descriptions. The dispersion curves for the effective medium (based on the assumption of $\beta a \ll 1$), though, become less and less accurate as β_n increases beyond ~0.8, as in Figs. 7 and 8. This behavior is very well confirmed by a detailed calculation, based on the Bloch–Floquet theorem in time and applied to an accurate model of the DTL. Just as frequency gaps are characteristic of spatial periodicity, β-gaps are a hallmark of temporal periodicity.

Fig. 12 illustrates the measured spectra of several signals transmitted all the way through the DTL for six externally launched traveling waves of frequency f, where the harmonics $f_M - f$ are present. The frequencies of the harmonics are 210 MHz $= (310-100)$ MHz, 200 MHz $= (310-110)$ MHz, 190 MHz $= (310-120)$ MHz, 170 MHz $= (310-140)$ MHz, and 160 MHz $= (310-150)$ MHz.

In continuation, we present another experimental result for the fabricated DTL. As is well known, when two frequencies f_1 and f_2 are nearly equal to each other, beats occur [24]. This phenomenon can be observed in many cases, being especially notable for sound. It follows from (16) that a DTL has a harmonic $f_M - f$ due to the temporal periodicity, as also described for a dynamic medium slab in [17]. For the externally launched traveling-wave signal of frequency f_1, the DTL generates another wave signal of frequency $f_2 = f_M - f_1$. Fig. 13 presents the interaction of these two signals for four cases of f_1 where beats can be appreciated. The beats of Fig. 13(a) have a frequency of 2 MHz corresponding to $|f_1 - f_2| = |154 - 156|$ MHz. The beats of Fig. 13(b)–(d) have frequencies $|153-157|$ MHz $= 4$ MHz, $|152-158|$ MHz $= 6$ MHz, and $|150-160|$ MHz $= 10$ MHz. These values correspond to a modulation frequency of $f_M = 310$ MHz and modulation $m = 0.25$.

IV. Conclusion

We have presented an in-depth study of EM wave propagation in a low-pass DTL, with the capacitors replaced by varactors that are modulated identically by an external voltage source that is periodic in time. We have designed and fabricated such a DTL with a frequency of modulation $f_M = 310$ MHz. A series of signal waves with frequencies f up to 305 MHz were launched and the corresponding propagation constants $\beta(\omega)$ were measured. The two bands $\beta_1(\omega)$ and $\beta_2(\omega)$ were obtained and these turn out to be separated by a bandgap $\Delta\beta$, provided that the modulation M of the dynamic capacitances $\tilde{C}(t)$ is sufficiently strong to overcome resistive effects ($M > M_R$).

We also showed that for waves of sufficiently large wavelength in comparison with the cell size of the DTL ($\beta a \lesssim 1$), the dispersion $\beta(\omega)$ can be well represented by a mean field theory. This provided that the permittivity $\varepsilon(t)$ of the effective medium is equal to the distributed capacitance $\tilde{C}(t)/a$ at every instant of time and that the permeability μ of this medium is equal to the distributed inductance L/a, neglecting damping effects.

We also demonstrated experimentally that for every working frequency f, the DTL generates harmonics $f_M - f$. In addition, we showed experimentally that the DTL generates beats for externally launched voltage signals of frequencies nearly equal to half of the modulation frequency.

APPENDIX
PROOF OF (15) AND OF $U_\Omega(t) \cong V_\Omega(t)$

Equation (9) can be written as

$$\begin{aligned}
&-4\sin^2(\beta a/2)v_N(t) - R[\tilde{C}(U_\Omega) + \tilde{C}'(U_\Omega)v_N(t)] \\
&\quad \times [\dot{U}_\Omega(t) + \dot{v}_N(t)] - RG_R[U_\Omega(t) + v_N(t)] \\
&\quad - LG_R[\dot{U}_\Omega(t) + \dot{v}_N(t)] - L\frac{d}{dt} \\
&\quad \times \{[\tilde{C}(U_\Omega) + \tilde{C}'(U_\Omega)v_N(t)][\dot{U}_\Omega(t) + \dot{v}_N(t)]\} \\
&= -\frac{R}{R_\Omega}V_\Omega(t) - \frac{L}{R_\Omega}\dot{V}_\Omega(t) \qquad \text{(A.1)}
\end{aligned}$$

where $(\cdot)$ means derivative with respect to time.

Now, we group together the terms proportional to $v_N(t)$, $\dot{v}_N(t)$, and $\ddot{v}_N(t)$ (neglecting the quadratic expressions) resulting in the following inhomogeneous differential equation:

$$\begin{aligned}
&[4\sin^2(\beta a/2) + R\tilde{C}'(U_\Omega)\dot{U}_\Omega(t) + RG_R \\
&\quad + L\tilde{C}''(U_\Omega)\dot{U}_\Omega^2(t) + L\tilde{C}'(U_\Omega)\ddot{U}_\Omega(t)]v_N(t) \\
&\quad + [R\tilde{C}(U_\Omega) + 2L\tilde{C}'(U_\Omega)\dot{U}_\Omega(t) + LG_R]\dot{v}_N(t) \\
&\quad + [L\tilde{C}(U_\Omega)]\ddot{v}_N(t) \\
&= (R/R_\Omega)V_\Omega(t) + (L/R_\Omega)\dot{V}_\Omega(t) - RG_RU_\Omega(t) \\
&\quad - [LG_R + R\tilde{C}(U_\Omega)]\dot{U}_\Omega(t) - L\tilde{C}(U_\Omega)\ddot{U}_\Omega(t) \\
&\quad - L\tilde{C}'(U_\Omega)\dot{U}_\Omega^2(t). \qquad \text{(A.2)}
\end{aligned}$$

Equation (A.2) has the form (N being arbitrary)

$$S(t)\frac{d^2v(t)}{dt^2} + T(t)\frac{dv(t)}{dt} + U(t)v(t) = F(t) \qquad (15)$$

where

$$\begin{aligned}
S(t) &= L\tilde{C}(U_\Omega) && \text{(A.3a)} \\
T(t) &= 2L\tilde{C}'(U_\Omega)\dot{U}_\Omega(t) + R\tilde{C}(U_\Omega) + LG_R && \text{(A.3b)} \\
U(t) &= 4\sin^2(\beta a/2) + L\tilde{C}'(U_\Omega)\ddot{U}_\Omega(t) + L\tilde{C}''(U_\Omega)\dot{U}_\Omega^2(t) \\
&\quad + RG_R + R\tilde{C}'(U_\Omega)\dot{U}_\Omega(t) && \text{(A.3c)} \\
F(t) &= -(R + Ld/dt)[\tilde{C}(U_\Omega)\dot{U}_\Omega(t) + G_RU_\Omega(t) \\
&\quad - (1/R_\Omega)V_\Omega(t)] && \text{(A.3d)}
\end{aligned}$$

where we used simple algebra to compactly rewrite the right-hand side of (A.2), namely, $F(t)$.

Now, as argued after (15), its solution mandates that $F(t) = 0$. Then it follows from (A.3d) that

$$\tilde{C}(U_\Omega)dU_\Omega/dt + G_RU_\Omega(t) - (1/R_\Omega)V_\Omega(t) = 0. \qquad \text{(A.4)}$$

We will not be concerned with a general solution for $U_\Omega(t)$ in terms of $V_\Omega(t)$. It suffices to say that the first term, which is on the order of $\Omega\tilde{C}U_\Omega(t)$, is negligible in comparison with the second term, because $\Omega\tilde{C} \ll G_R$ under standard experimental conditions. In addition, $G \ll 1/R_\Omega$, so that $G_R \cong 1/R_\Omega$. Hence, (A.4) simply reduces to

$$U_\Omega(t) \cong V_\Omega(t). \qquad \text{(A.5)}$$

This implies that in (A.3a)–(A.3c), and thus (15), the voltage $U_\Omega(t)$ can be replaced by the modulation voltage $V_\Omega(t)$ to a very good approximation.

ACKNOWLEDGMENT

Author J. R. Reyes-Ayona would like to thank Prof. J. R. Zurita-Sánchez, Prof. J. L. Olvera-Cervantes, and Prof. A. Corona-Chávez of INAOE for helpful discussions regarding various aspects of this paper, and Prof. I. Zaldívar-Huerta for the help with the laboratory equipment.

REFERENCES

[1] A. L. Cullen, "A travelling-wave parametric amplifier," *Nature*, vol. 181, no. 4605, p. 332, Feb. 1958.

[2] E. S. Cassedy, "Temporal instabilities in traveling-wave parametric amplifiers," *IRE Trans. Microw. Theory Techn.*, vol. MTT-10, no. 1, pp. 86–87, Jan. 1962.

[3] E. S. Cassedy and A. A. Oliner, "Dispersion relations in time-space periodic media: Part I—Stable interactions," *Proc. IEEE*, vol. 51, no. 10, pp. 1342–1359, Oct. 1963.

[4] E. S. Cassedy, "Dispersion relations in time-space periodic media part II—Unstable interactions," *Proc. IEEE*, vol. 55, no. 7, pp. 1154–1168, Jul. 1967.

[5] E. S. Cassedy, "Waves guided by a boundary with time-space periodic modulation," *Proc. Inst. Elect. Eng.*, vol. 112, no. 2, pp. 269–279, Feb. 1965.

[6] O. J. Downing and P. A. Watson, "Active and passive broadbanding of parametric amplifiers," *Proc. Inst. Elect. Eng.*, vol. 120, no. 6, pp. 629–636, Jun. 1973.

[7] J. J. Harris and J. M. Woodcock, "Low noise GaAs varactor and mixer diodes prepared by molecular beam epitaxy," *Electron. Lett.*, vol. 16, no. 9, pp. 317–319, Apr. 1980.

[8] A.-S. Porret, T. Melly, C. C. Enz, and E. A. Vittoz, "Design of high-Q varactors for low-power wireless applications using a standard CMOS process," *IEEE J. Solid-State Circuits*, vol. 35, no. 3, pp. 337–345, Mar. 2000.

[9] S. Ranganathan and Y. Tsividis, "Discrete-time parametric amplification based on a three-terminal MOS varactor: Analysis and experimental results," *IEEE J. Solid-State Circuits*, vol. 38, no. 12, pp. 2087–2093, Dec. 2003.

[10] W. Lee and E. Afshari, "Distributed parametric resonator: A passive CMOS frequency divider," *IEEE J. Solid-State Circuits*, vol. 45, no. 9, pp. 1834–1844, Sep. 2010.

[11] S. Qin, Q. Xu, and Y. E. Wang, "Nonreciprocal components with distributedly modulated capacitors," *IEEE Trans. Microw. Theory Techn.*, vol. 62, no. 10, pp. 2260–2272, Oct. 2014.

[12] A. B. Kozyrev, H. Kim, and D. W. van der Weide, "Parametric amplification in left-handed transmission line media," *Appl. Phys. Lett.*, vol. 88, no. 26, pp. 264101-1–264101-3, Jun. 2006.

[13] A. B. Kozyrev and D. W. van der Weide, "Nonlinear left-handed transmission line metamaterials," *J. Phys. D, Appl. Phys.*, vol. 41, no. 17, pp. 173001-1–173001-10, Aug. 2008.

[14] L. Q. English *et al.*, "Generation of localized modes in an electrical lattice using subharmonic driving," *Phys. Rev. Lett.*, vol. 108, pp. 084101-1–084101-5, Feb. 2012.

[15] M. Gorkunov and M. Lapine, "Tuning of a nonlinear metamaterial band gap by an external magnetic field," *Phys. Rev. B, Condens. Matter,* vol. 70, pp. 235109-1–235109-9, Dec. 2004.

[16] P. Halevi, U. Algredo-Badillo, and J. R. Zurita-Sánchez, "Optical response of a slab with time-periodic dielectric function ε(t): Towards a dynamic metamaterial," *Proc. SPIE*, vol. 8095, pp. 80950I-1–80950I-15, Sep. 2011.

[17] J. R. Zurita-Sánchez, P. Halevi, and J. C. Cervantes-González, "Reflection and transmission of a wave incident on a slab with a time-periodic dielectric function ε(t)," *Phys. Rev. A, Gen. Phys.,* vol. 79, no. 5, pp. 053821-1–053821-13, May 2009.

[18] J. R. Reyes-Ayona and P. Halevi, "Observation of genuine wave vector (k or β) gap in a dynamic transmission line and temporal photonic crystals," *Appl. Phys. Lett.*, vol. 107, no. 7, pp. 074101-1–074101-3, Aug. 2015.

[19] J. R. Zurita-Sánchez and P. Halevi, "Resonances in the optical response of a slab with time-periodic dielectric function ε(t)," *Phys. Rev. A, Gen. Phys.,* vol. 81, no. 5, pp. 053834-1–053834-9, May 2010.

[20] J. R. Zurita-Sánchez, J. H. Abundis-Patiño, and P. Halevi, "Pulse propagation through a slab with time-periodic dielectric function ε(t)," *Opt. Exp.*, vol. 20, no. 5, pp. 5586–5600, Feb. 2012.

[21] M. Ershov, H. C. Liu, L. Li, M. Buchanan, Z. R. Wasilewski, and A. K. Jonscher, "Negative capacitance effect in semiconductor devices," *IEEE Trans. Electron Devices*, vol. 45, no. 10, pp. 2196–2206, Oct. 1998.

[22] C. Kittel, *Introduction to Solid State Physics*, 8th ed. Hoboken, NJ, USA: Wiley, 1985, pp. 176–180.

[23] A. Corona-Chavez, J. R. R. Ayona, D. V. B. Murthy, and J. L. O. Cervantes, "Miniaturized forced-mode ring resonator with capacitive loading," *Prog. Electromagn. Res. Lett.*, vol. 31, pp. 65–73, Apr. 2012.

[24] J. P. Den Hartog, *Mechanical Vibrations*, 1st ed. New York, NY, USA: Dover, 1985, pp. 5–7.

José Roberto Reyes-Ayona received the B.Sc. degree in electronics from the Benemérita Universidad Autónoma de Puebla, Puebla, Mexico, in 2001, and the M.Sc. and D.Sc. degrees in electronics from the National Institute of Astrophysics, Optics and Electronics, Cholula, Mexico, in 2010 and 2015, respectively.

He is currently an Associate Professor with the Universidad de Guanajuato, Salamanca, Mexico. His current research interests include transmission lines and microwave technology.

Peter Halevi received the D.Sc. degree in physics from the Technion–Israel Institute of Tecnology, Haifa, Israel, in 1969.

He held several positions with McGill University, Montréal, QC, Canada, the Benemérita Universidad Autónoma de Puebla, Puebla, Mexico, the University of California at Irvine, Irvine, CA, USA, the Weizmann Institute of Science, Rehovot, Israel, and the Centre National de la Recherche Scientifique, Grenoble, France. He is currently with the National Institute of Astrophysics, Optics and Electronics, Cholula, Mexico. His current research interests include the aspects of wave phenomena in solids, photonic crystals, phononic crystals and, recently, the transmission lines.